Int J Adv Manuf Technol (1997) 13:677–684

The International Journal of
Advanced Manufacturing Technology

A Geometrical Model of the Cut in Five-Axis Milling Accounting for the Influence of Tool Orientation

E. Agson Gani, J. P. Kruth, P. Vanherck and B. Lauwers

Production Engineering, Machine Design and Automation Division, Department of Mechanical Engineering, Katholieke Universiteit Leuven, Belgium

This paper presents a model of the cut geometry in five-axis milling. This allows the establishment of a better model of cutting force to account for the influence of the tool orientation. The formulation of the width and the thickness of the cut were derived and implemented in a computer simulation. The results of simulations were verified experimentally and a good agreement was obtained. The result shows the importance of including the influence of the tool orientation in the cut cross-section calculation.

Keywords: Cut geometry; Cutting force; Five-axis milling; Tool orientation

1. Introduction

The surface characteristics of milled surfaces by five-axis milling have been studied by taking into account the influence of tool orientation. The investigation verifies that the influence of lead angle both on surface accuracy and roughness is significant [1–3].

One of the significant influences on the surface accuracy is the surface deviation due to the finite stiffness of machine and/or tool system as shown on Fig. 1. This phenomenon occurs because the lead angle influences the cutting force, as well as the compliance of the structure loop from workpiece to the tool tip.

Following the Kienzle theorem, the cutting force is a function of the cross-section area of the cut [4]. Actually, the cross-cut area in five-axis milling depends on the tool orientation applied during cutting [2]. Although various researchers [5–8] have presented a series of papers about the mechanistic model for cutting force in milling, most of the existing models are dedicated to three-axis (basic) milling. Some specific parameters in five-axis milling that have a major influence on the cutting force have not been taken into account.

Correspondence and offprint requests to: E. Agson Gani, PMA Division, Department of Mechanical Engineering, Katholieke Universiteit Leuven, Celestijnenlaan 300 B, 3001-Belgium

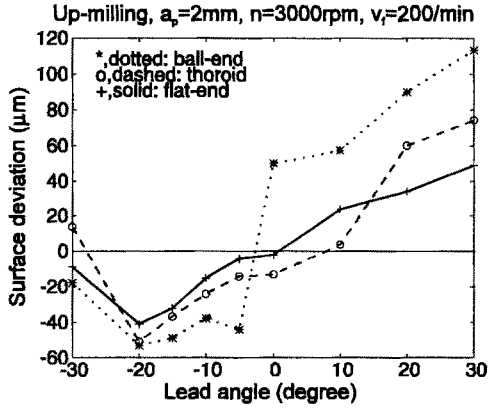

Fig. 1. Surface deviation versus lead angle.

Because of this, a knowledge of the cut geometry as a function of tool orientation is essential in order to be able to predict the cutting force in five-axis milling. The aim of this work is to study the cut geometry in five-axis milling, taking into account the influence of the tool orientation as a basis on which a more reliable cutting force model is built.

2. Ball-end Versus Flat-end Cutters

One of the critical problems in five-axis milling is the positioning of the cutter in relation to the surfaces in order to machine without having overcut or undercut (gouging). Because of this problem, ball-end cutters are preferred. Overcutting does not cause a big problem when using ball-end cutters. The calculation of the NC tool path for ball-end cutters is mainly a problem of surface offset.

An important drawback of ball-end cutters is the varying cutting speed along the tool radius. The maximal cutting speed v_c is reached on the tool diameter, and at the tool tip v_c is zero (see Fig. 2(*b*)). This leads to cutting edge chipping as well as poor surface roughness.

In order to avoid these problems, a specified lead or/and tilt angle can be used, instead of perpendicular cutting conditions.

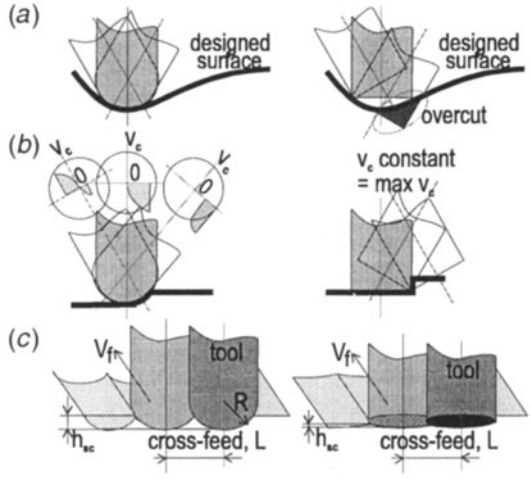

Fig. 2. Ball versus flat-end cutters, (*a*) gouging, (*b*) cutting speed, (*c*) scallop height.

However, this method is only advantageous for machining highly curved surfaces. To machine low-curvature surfaces, a flat-end cutter is more advantageous. This method enables a smaller number of cutting passes to be used and as a result a shorter machining time is needed [9,10].

Because of this, this study focuses on milling using a flat-end cutter. Additionally, when five-axis milling is used to machine a sculptured surface with flat-end cutters, the tool orientation can be controlled by either a lead or a tilt angle. However, machining using a tilt angle will produce a higher scallop height or longer machining time. A tilt angle is normally used only for collision avoidance when machining a high-curvature surface. Therefore, this study only takes the lead angle as a parameter to study.

Actually, since the cut geometry with ball-end cutters always occurs on a spherical cap, the cut geometry does not vary as a function of tool orientation. The influences of the tool orientation on the engagement parameters when using ball-end cutters have been investigated [11].

3. Geometry of the Cut in Basic Milling

Following the ISO/DIS 3002/3 standard, the cut is defined as a layer of the workpiece material to be removed by a single action of a cutting part [12]. There are three main components of the cut, i.e. nominal cross-section area of the cut (A), nominal width of cut (b), nominal thickness of cut (h).

The geometrical model of the cut in this study is developed based on the cut geometry of a basic (three-axis) milling process. An identical cut geometry occurs in five-axis milling when the tool is perpendicular to the milled surface, i.e. when the tool orientation is zero (see Fig. 3).

From Fig. 3, basic formulations can be deduced as follows:

$$h = AA' \sin \chi \cos \lambda$$

since $AA' = f_z \sin \varphi$, then:

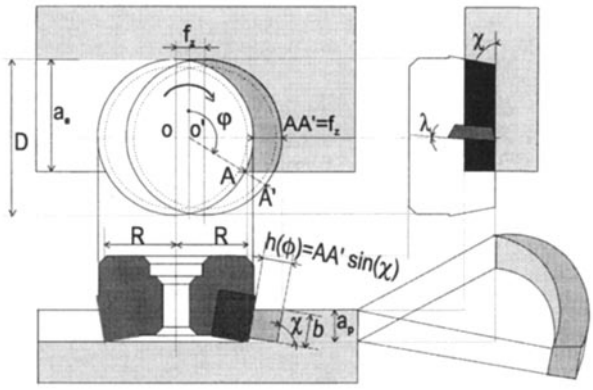

Fig. 3. Basic form of cut geometry.

$$h(\varphi) = f_z \sin \chi \cos \lambda \sin \varphi \tag{1}$$

$$b = \frac{a_p}{\sin \chi \cos \lambda} \tag{2}$$

where h = the cut thickness (mm)
b = the cut width (mm)
f = feed rate (mm per tooth)
a_p = axial depth of cut (mm)
χ = tool cutting edge angle (degree)
ω = feed motion angle (degree)
λ = helical angle (degree)

This study uses flat-end cutters with inserts that are characterised by a small helical angle. Therefore, in the next analysis the helical angle will be ignored in order to simplify the problem.

Another parameter relating to the cut geometry is the feed motion angle (φ). This angle is defined as the angle between the directions of the simultaneous feed motion and primary motion measured in the working plane P_{fe}. This parameter is used to locate the instantaneous cross-cut area along the tool/workpiece engagement or cut length (Fig. 4). This parameter is bounded by a certain value (φ_{min} and φ_{max}) that depends on the conditions of tool–workpiece engagement.

There are two extreme conditions of tool engagement, affected by the radial depth of cut (a_e), and the tool radius (R). In the first case, the axis of the tool is outside the cut, while in the second case, the axis is inside the cut. For the first case (Fig. 4),

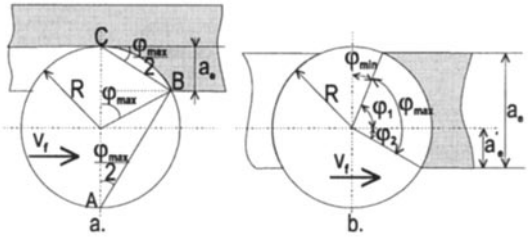

Fig. 4. Tool-workpiece engagement.

$$\varphi_{min} = 0$$

$$\varphi_{max} = \arccos\left(\frac{R - a_e}{R}\right) \tag{3}$$

and for the second case (Fig. 4*b*),

$$\varphi_{min} = \arccos\left(\frac{a_e - a'_e}{R}\right)$$

$$\varphi_{max} = \arcsin\left(\frac{a'_e}{R}\right) + \arcsin\left(\frac{a_e - a'_e}{R}\right) \tag{4}$$

4. Cut Geometry for Positive Lead Angle

In the previous section, on milling with a tool perpendicular to the milled surface, only the nominal thickness of cut varies as a function of the feed motion angle. However, by applying a lead angle β_f, the depth of cut will also vary. For the case of using a positive lead angle, the cut geometry can be classified into two categories.

4.1 Positive Lead Angle, $0° < \beta_f \leq \arcsin(a_p/R)$

The general view of the cut geometry in this case is depicted in Fig. 5. In this case, the depth of the cut varies from $a_p - R\sin\beta_f$ at $\varphi = 0°$ to a_p at $\varphi = 90°$, and the path shape of the tool on the workpiece is not circular any more. It becomes an

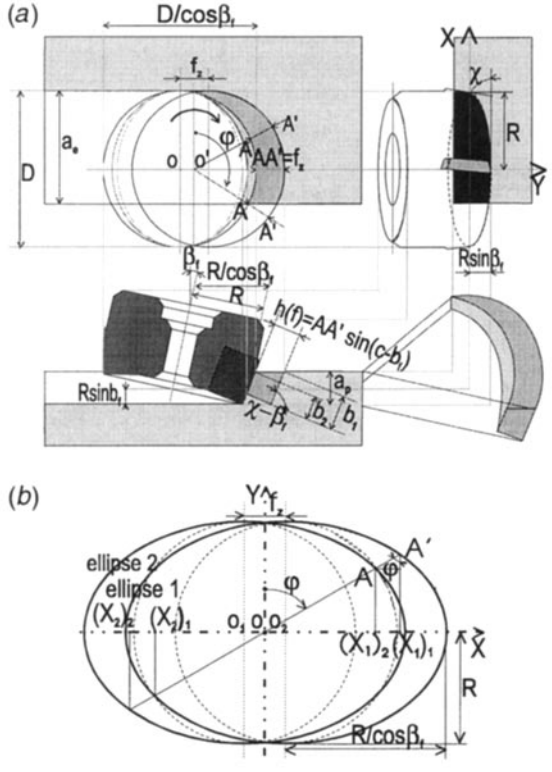

Fig. 5. Lead angle positive, $0° < \beta_f \leq \arcsin(a_p/R)$. (*a*) General view. (*b*) Detailed top view of path form of tool.

ellipse with a long axis equal to $R/\cos\beta_f$ oriented along the feed direction (lead angle direction) and a short axis equal to R (Fig. 5). As a consequence, the relation between the instantaneous cut thickness and the feed motion angle is not as simple as when milling with a zero tool-inclination angle.

The instantaneous cut thickness is derived based on the equation of the ellipse on Fig. 5(*b*),

$$\frac{X^2}{R^2/\cos^2\beta_f} + \frac{Y^2}{R^2} = 1$$

or,

$$\cos^2\beta_f X^2 + Y^2 = R^2$$

The equation of the first ellipse is obtained by shifting the X origin to $f_z/2$,

$$\cos^2\beta_f \left(X - \frac{1}{2}f_z\right)^2 + Y^2 = R^2 \tag{5}$$

if $Y = \cot\varphi\, X$ is substituted into equation (5),

$$(\cos^2\beta_f + \cot^2\varphi)X^2 - (f_z\cos^2\beta_f)X + \left(\frac{1}{2}f_z\right)^2\cos^2\beta_f - R^2 = 0 \tag{6}$$

From equation (6), we get the value of $(X_1)_1$ and $(X_2)_1$ that are the short and the long abscissae of the first ellipse, respectively. The $(X_1)_2$ and $(X_2)_2$ values for the second ellipse can be found in a similar way by shifting its X origin to $-(f_z/2)$. The difference between $(X_1)_1$ and $(X_1)_2$ is used to calculate the instantaneous cut thickness (Fig. 5(*b*)).

$$AA' = \frac{(X_1)_1 - (X_1)_2}{\sin\varphi} \tag{7}$$

The differences of abscissa length between two consecutive ellipses $(X_1)_1 - (X_1)_2$ can be solved by solving the second-order equation (6). This yields:

$$(X_1)_1 - (X_1)_2 = \frac{f_z\cos^2\beta_f\sin^2\varphi}{\cos^2\beta_f\sin^2\varphi + \cos^2\varphi}$$

$$(7) \Rightarrow AA' = \frac{f_z\cos^2\beta_f\sin\varphi}{\cos^2\beta_f\sin^2\varphi + \cos^2\varphi} \tag{8}$$

since $h(\varphi) = AA'\sin(\chi - \beta_f)$, then:

$$h(\varphi) = \frac{f_z\cos^2\beta_f\sin(\chi - \beta_f)\sin\varphi}{\cos^2\beta_f\sin^2\varphi + \cos^2\varphi} \tag{9}$$

As mentioned before, by applying a lead angle not equal to zero, the depth of cut varies as a function of the feed motion angle (φ). The formula for this relationship can be deduced from the ellipse on the bottom of tool on the right-hand side view of Fig. 5(*a*).

$$Y = \frac{b}{a}\sqrt{(a^2 - X^2)}$$

where $a = R$, $b = R\sin\beta_f$, and $X(\varphi) = R\cos\varphi$, it yields:

$$Y(\varphi) = \frac{R\sin\beta_f}{R}\sqrt{(R^2 - R^2\cos^2\varphi)}$$

$$Y(\varphi) = R\sin\beta_f\sin\varphi \tag{10}$$

From Fig. 5(*a*) we also get the instantaneous depth of cut,

$$a_p(\varphi) = a_p - R\sin\beta_f + Y(\varphi)$$

$$a_p(\varphi) = a_p - R\sin\beta_f + R\sin\beta_f \sin\varphi \quad (11)$$

By applying a tool orientation, the difference between the inner and the outer cut width becomes greater, where for the outer side,

$$b_1(\varphi) = \frac{a_p - R\sin\beta_f + R\sin\beta_f \sin\varphi}{\sin(\chi - \beta_f)} \quad (12)$$

for the inner side,

$$b_2(\varphi) = b_1(\varphi) - AA'\cos(\chi - \beta_f)$$

by substituting the value AA' from (8), we get:

$$b_2(\varphi) = \frac{a_p - R\sin\beta_f + R\sin\beta_f \sin\varphi}{\sin(\chi - \beta_f)}$$

$$-f_z \cos^2\beta_f \cos(\chi - \beta_f)\sin\varphi \cos^2\beta_f \sin^2\varphi + \cos^2\varphi \quad (13)$$

Since the shape of the cross-cut area is a trapezium, therefore for practical purposes, it is simpler to use an average cut width (b_m). The average cut width is defined as the average value of the inner and outer cut width.

$$b_m(\varphi) = \frac{b_1(\varphi) + b_2(\varphi)}{2}$$

$$b_m(\varphi) = \frac{a_p - R\sin\beta_f + R\sin\beta_f \sin\varphi}{\sin(\chi - \beta_f)} - \frac{f_z \cos^2\beta_f \cos(\chi - \beta_f)\sin\varphi}{2(\cos^2\beta_f \sin^2\varphi + \cos^2\varphi)} \quad (14)$$

4.2 Positive Lead Angle, arc $\sin(a_p/R) < \beta_f < 90°$

The second type of the cut geometry for a positive lead angle occurs by applying a lead angle lying between arc $\sin(a_p/R)$ and 90°. There are two main differences in the cut geometry in this case compared to the previous one. First, the value of $R\sin\beta_f$ is greater than a_p. As a result, the cut width does not start from a certain non-zero value, but starts from zero to the maximum value. The second is that the effective radial depth of cut ($a_{e\,eff}$) is not always equal to the programmed radial depth of cut (a_e) or pick-feed. The $a_{e\,eff}$ decreases for increasing lead angle. The value of $a_{e\,eff}$ depends on the effective tool contact radius with the workpiece. The effective tool contact radius itself is a function of the lead angle (β_f), tool radius (R), and a_p as follows (Fig. 6):

$$R_{eff} = \sqrt{\left(\frac{2a_pR\sin\beta_f - a_p^2}{\sin^2\beta_f}\right)} \quad (15)$$

and,

$$a_{e_{eff}} = a_e - R + \sqrt{\left(\frac{2a_p R\sin\beta_f - a_p^2}{\sin^2\beta_f}\right)} \quad (16)$$

Although the effective radial depth of cut is not equal to the programmed one, the cut thickness and width can still be calculated in a similar way to the previous case. However, the value of the effective radial depth of cut has to be considered for the calculation of the boundary of the feed motion angle (φ).

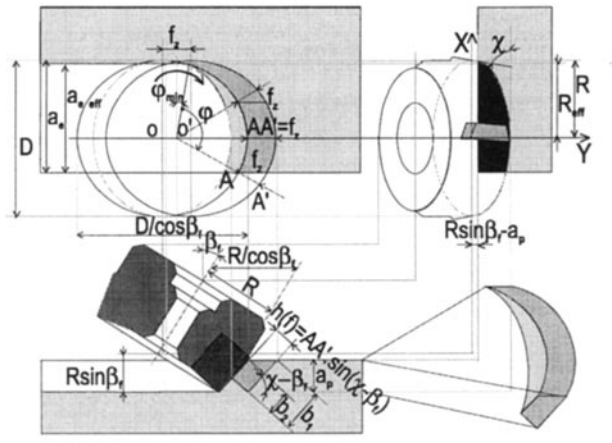

Fig. 6. Lead angle positive, arcsin $(a_p/R) < \beta_f < 90°$.

5. Cut Geometry for Negative Lead Angle

5.1 Negative Lead Angle, $-\text{arc}\sin(a_p/D) < \beta_f < 0°$

As illustrated in Fig. 7, the cut geometry in this case is quite complex. This is because, the tool contacts the work surface not only on the front side of its periphery (major cutting edge S) and its bottom (minor cutting edge S'), but it also contacts the work surface with the back side of its bottom. In order to simplify the problem, the cuts that contact with the periphery of cutter and the bottom of the cutter will be treated independently (see Fig. 7(*b*)).

First, let us consider the cut that contacts with the periphery of the cutter (the major cut). The formula of the major cut geometry can be derived in a similar way to when using a positive lead angle.

Further, as shown in Fig. 7(*b*)), the shape of the cut that contacts with the bottom of the cutter (minor cut) is a cylinder with a radius equal to the radius of the cutter, and a height equal to b_3. Notice that, depending on the width of the insert cutter and the tool cutting edge angle χ, the minor cut might not extend to the centre of this cylinder. The value of b_3 equals:

$$b_3 = f_z \sin\beta_f \quad (17)$$

Actually, the value of the cylinder radius with respect to the point O varies as a function of the feed motion angle, such that:

$$R(\varphi)_{12} = -\tfrac{1}{2}(f_z\sin\varphi) \pm \sqrt{\left(R^2 - \tfrac{1}{4}f_z^2\cos^2\varphi\right)} \quad (18)$$

However, as $f_z \ll R$, this equation can be simplified as $R(\varphi) = R$. This simplified value of R is used to calculate the instantaneous thickness of the minor cut.

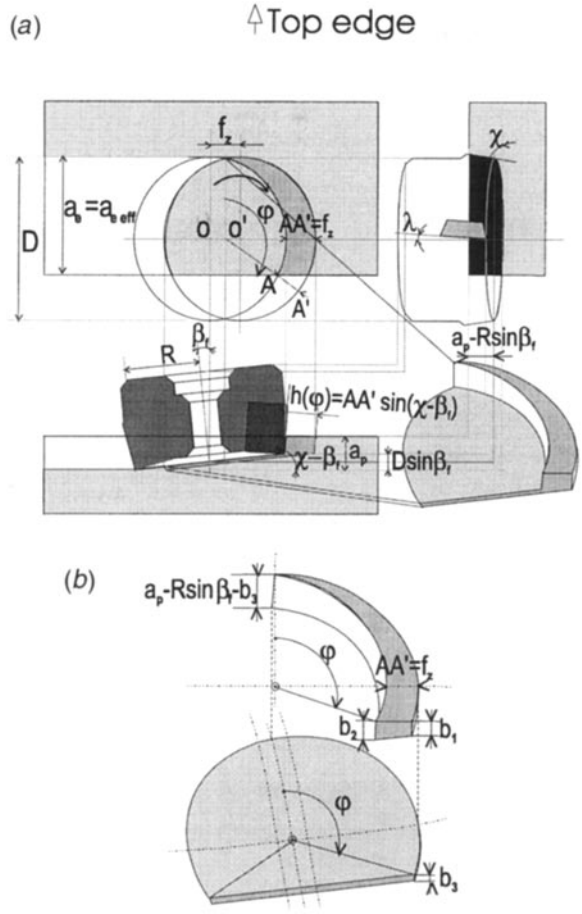

Fig. 7. Negative lead angle, $-\arcsin(a_p/D) < \beta_f < 0°$. (*a*) General view. (*b*) Separated cut detailed figure.

Further, considering the type of tool–workpiece engagement, the thickness of the minor cut can be expressed as a function of the instantaneous contact angle as follows.

For the case when the axis of the tool is outside the cut,

$$h(\varphi)=\begin{cases} R-\dfrac{R-a_e}{\cos\varphi} & \text{for } 0° \le \varphi \le \varphi_1 \\ 0 & \text{for } \varphi_1 < \varphi < 360° - \varphi_2 \\ R-\dfrac{R-a_e}{\cos\varphi} & \text{for } 360° - \varphi_2 < \varphi < 360° \end{cases} \tag{19}$$

where; $\varphi_1 \approx \varphi_2 \approx \arccos\left(\dfrac{R-a_e}{R}\right)$

For the case that the axis of the tool is inside the cut,

$$h(\varphi)=\begin{cases} R & \text{for } 0° \le \varphi \le \varphi_1 \\ \dfrac{a_e - R}{\sin(\varphi-90°)} & \text{for } \varphi_1 < \varphi < 360° - \varphi_2 \\ R & \text{for } 360° - \varphi_2 < \varphi < 360° \end{cases} \tag{20}$$

where; $\varphi_1 \approx \varphi_2 \approx \arcsin\left(\dfrac{a_e-R}{R}\right) + 90°$

5.2 Negative Lead Angle, $-\arcsin(a_p/R) < \beta_f \le -\arcsin(a_p/D)$

The illustration of the cut in this case is depicted in Fig. 8. This figure shows that the cut in this case is almost similar to the previous one, but the boundary of the feed motion angle is slightly different. This is because the depth of cut a in this case is smaller than $D\sin\beta_f$.

As a result, although the contact mode between the cutters and the workpiece is still the same as in the previous case, there is a part of the front side of the cutter that is no longer in contact with the work surface.

As shown on Fig. 8, four different cases of tool–workpiece engagement can be considered depending on the value of a_e, R, φ_1, φ_2, and φ_3. Here, φ_1 is a limit of the feed motion angle when the cutter periphery still contacts the work surface. The formulation of this parameter is:

$$\varphi_1 = \arcsin\left(\frac{a_p}{R\sin\beta_f} - 1\right) \tag{21}$$

5.3 Negative Lead Angle, $-90° < \beta_f \le -\arcsin(a_p/R)$

In this case, $R\sin\beta_f$ is larger than a_p. As a result, the cutter contacts the work surface only with the back side of its bottom. The cut geometry of this case becomes simpler as illustrated on Fig. 9.

This figure shows that the shape of the cut is a part of a cylinder, bounded by some values of the feed motion angle and with a constant height. However, the radius of the cylinder varies as a function of the feed motion angle, depending on the cutter–workpiece engagement condition.

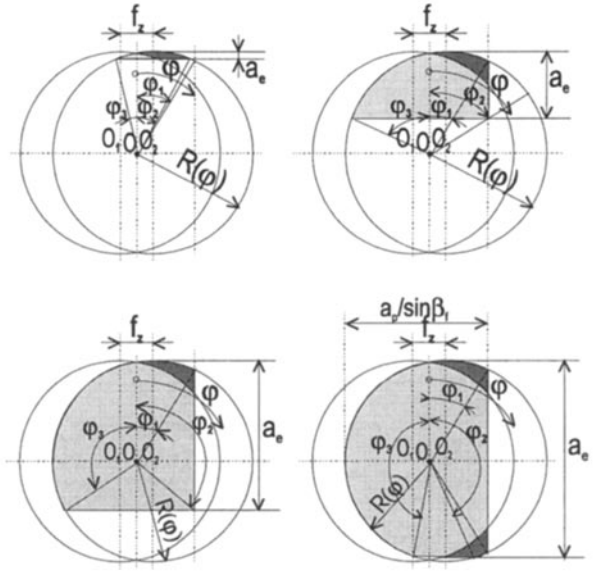

Fig. 8. Negative lead angle, $-\arcsin(a_p/R) < \beta_f \le -\arcsin(a_p/D)$. (*a*) $a_e <= R - R\cos\varphi_1$; (*b*) $R - R\cos\varphi_1 < a_e <= R$; (*c*) $R < a_e <= D - R\cos\varphi_1$; (*d*) $D - R\cos\varphi_1 < a_e <= D$.

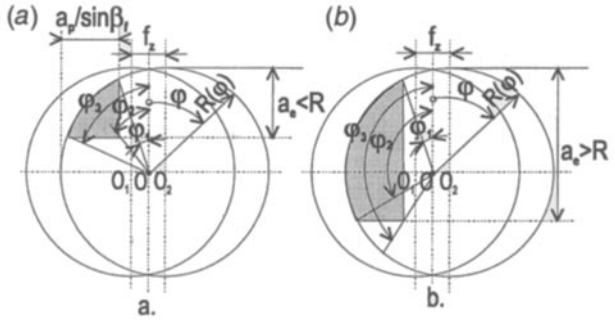

Fig. 9. Negative lead angle, $-90° < \beta_f \leq -\arcsin(a_p/R)$.

6. Influence of Scallop to the Cut Geometry

The scallop profile is the most substantial component of the surface roughness in five-axis milling. It is measured perpendicular to the feed direction. This profile is produced as the tool, with a certain tool inclination, moves on the surface following parallel tracks. The resulting surface roughness is much larger than the roughness measured parallel to the direction of feed. More details of the surface characteristics of five-axis milling including the influence of the tool orientation are outlined in [3].

The scallop profile is mainly characterised by the scallop height, defined as the height of the peaks left on the surface after machining with respect to the deepest points of the milled grooves. The scallop height is mainly a function of tool geometry, cross-feed, tool inclination, and surface geometry. When machining a flat surface with flat-end cutters, the theoretical relationship is:

$$h_{sc\ flat\text{-}end} = \sin \beta_f \left(R - \sqrt{R^2 - (L/2)^2}\right) \tag{22}$$

where h_{sc} = scallop height

L = cross-feed (pitch) $\leq 2\ r_{eff}$

Figure 10 shows a surface with two consecutive milling paths milled with a positive lead angle and a radial depth of cut (a_e) smaller than R. This figure gives an illustration of the influence of the scallop profile on the actual and the previous milling path on the cut geometry. It shows that the actual

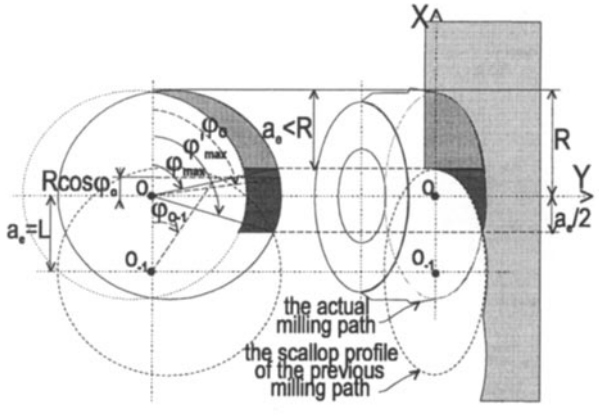

Fig. 10. Influence of scallop height to the cut geometry.

radial depth of cut is no longer equal to the cross-feed (L), but is equal to $R + (L/2)$. This situation changes the angle of the cutter–workpiece engagement. As a consequence, the maximum value of the feed motion angle, where the cutter is still in contact with the work surface, changes from φ_{max} as given in (3) or (4) to,

$$\varphi'_{max} = \arcsin\left(\frac{a_e/2}{R}\right) + 90° \tag{23}$$

For the feed motion angles in the range φ_{max} to φ'_{max}, the value of the cut thickness still can be calculated using formula (9). However, the value of the cut width in this range of φ should be calculated using another formula for the axial depth of cut. The formula of the axial depth of cut in this range of φ can be deduced from the equation of the ellipse of the bottom of the cutter in the right-hand side view of the Fig. 10 as follows:

$$a_{p(\varphi_{max} \div \varphi'_{max})} = Y_{(0)} - Y_{(0-1)} \tag{24}$$

where, $Y_{(0)}$ and $Y_{(0-1)}$ are the ordinate of the ellipse of the actual and the previous scallop profile respectively. From (10):

$$Y_{(0)} = R \sin \beta_f \sin \varphi$$

$$Y_{(0-1)} = R \sin \beta_f \sin \varphi_{(0-1)}$$

By substituting these equations into equation (24):

$$a_{p(\varphi_{max} \div \varphi'_{max})} = R \sin \beta_f (\sin \varphi_0 - \sin \varphi_{(0-1)}) \tag{25}$$

Since the value of the cut and the cutting force depends only on φ_0, therefore the value of $\varphi_{(0-1)}$ should be related to the value of φ_0. From the top view of Fig. 10, it can be deduced that for $\varphi_{max} < \varphi_0 < \varphi'_{max}$:

$$\varphi_{(0-1)} = \arccos\left(\frac{a_e + R\cos \varphi_0}{R}\right) \tag{26}$$

By substituting equation (26) into (25),

$$a_{p(\varphi_{max} \div \varphi'_{max})} = R \sin \beta_f \left(\sin \varphi_0 - \sin\left(\arccos\left(\frac{a_e + R\cos\varphi_0}{R}\right)\right)\right) \tag{27}$$

The formulation for the other cases can be derived in a similar way. However, in the case of a negative lead angle, the influence of the previous scallop profile should be considered only on the back side of the minor cutting edge.

7. Simulation and Experimental Results

Based on the formulae derived in the previous sections, a simulation program using MATLAB has been created, enabling the calculation of the cut geometry for a given lead angle. Some results of the simulation program are depicted on Fig. 11. By comparing the graphs in Figs 11(b) and 11(c) to the graphs in Fig. 11(a) ($\beta_f = 0°$), it can be seen that the lead angle has a significant influence on the cut geometry

Cutting tests were performed to verify this model using single insert cutters HM-K15 diameter 20 mm on Aluminium AlMgSi1. The tests were done with a cutting speed 3000 r.p.m.,

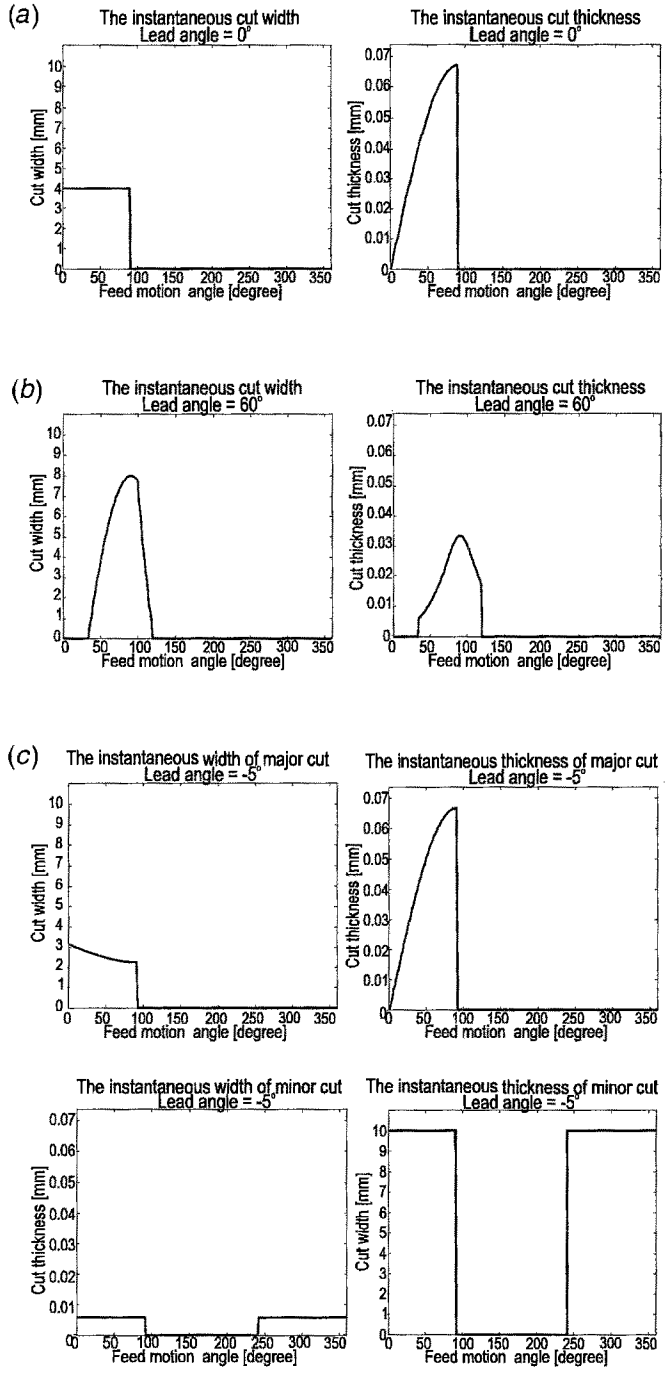

Fig. 11. Simulated of the cut geometry. (*a*) Lead angle $\beta_f = 0°$, (*b*) 60°, (*c*) −5°.

$a_p = 4$ mm, $a_e = 10$ mm, and $f_z = 0.067$ mm/teeth. The pictures of chips, and the tangential cutting force resulting from these tests are depicted in Fig. 12. Measurement of the cutting force is done with a piezo-electric dynamometer KISTLER type 9259.

A comparison of the graphs in Figs 11 and 12 indicates a good agreement with the tangential cutting force obtained by simulation and the measured value. After taking the compression ratio into account, a good agreement is obtained by

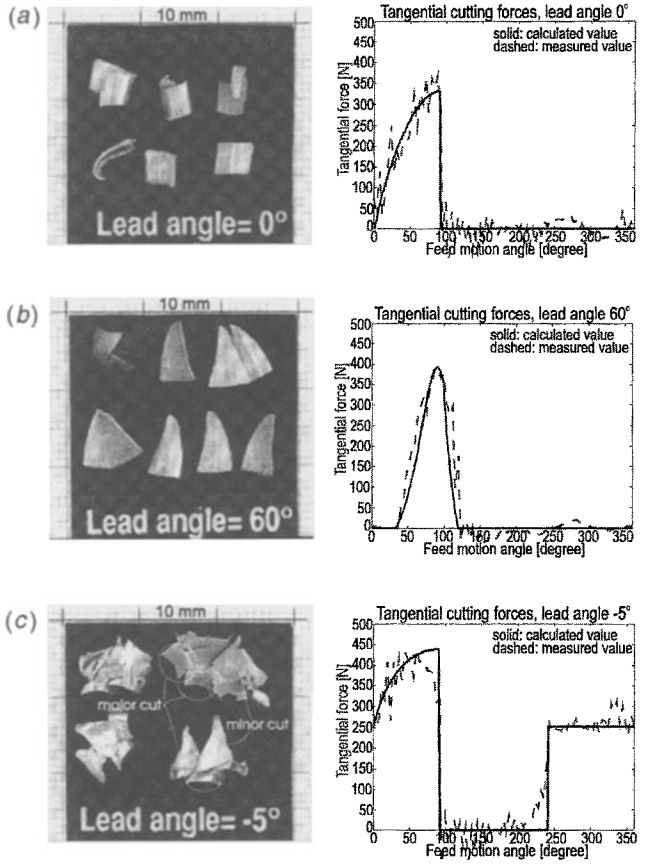

Fig. 12. Photographs of chips, and comparison graphs of simulation and experimental cutting forces. (*a*) Lead angle $\beta_f = 0°$, (*b*) 60°, (*c*) −5°.

comparing the chip geometry (the width for the major cut and the thickness for the minor cut) resulting from the cutting test as shown in the figures with the simulated cut dimension.

8. Conclusion

The influence of tool orientation (lead angle) on the cut geometry in five-axis milling has been studied. The formulation of the width and the thickness of cut were derived, and used for computer simulation. The results of the simulation were verified experimentally and a good agreement was reached.

The results show that the tool inclination in five-axis milling has a large influence on the cut cross-section and hence on the cutting forces, on the chatter, and on the product accuracy. As a consequence, proper selection of cutting parameters should take those effects into account.

Todays CAM software for five-axis milling does not take those influences into account to complement the geometrical constraints governing tool inclination. The paper presents algorithms that allows the introduction of those elements in five-axis NC programming systems.

As an example, even if the selected depth of cut is the same, applying a higher positive lead angle will produce a higher width of cut (Fig. 11). Actually, the width of the cut

is limited by the value that is called "chatter depth" (cut width when chatter arises) [13]. As occurred in the cutting tests carried-out to verify the present model, chatter-marks are produced when milling with a lead angle of 50° or higher.

Acknowledgement

This research is sponsored by the Belgian programme on Inter-University Attraction Poles by the Belgian State, Prime Minister's Office, Science Policy Programming (IUAP-50).

E.A.G. is a researcher of the Machine-tool, Production technique, and Automation laboratory (MEPPO), and an engineering staff member of Nusantara Aircraft Industry Indonesia. He is currently pursuing a PhD program at Katholieke Universiteit Leuven under the supervision of Professor J. P. Kruth with a scholarship from PT. PAL, Indonesia. He would like to thank those institutions for giving him this opportunity.

References

1. E. Agson Gani, "An investigation of the surface characteristics on five axis milling process using toroid cutter", Master thesis, Engineering Faculty, K.U. Leuven, 1991.
2. E. Agson Gani, B. Lauwers, P. Klewais and J. Dehaes, "An investigation of the surface characteristics in five axis milling with toroid cutter, *Proceedings, Pacific Conference on Manufacturing (PCM '94), Jakarta, Indonesia, 19–22 December*, pp. 53–60, 1994.
3. E. Agson Gani, J. P. Kruth and B. Lauwers, "A study of the influence of the tool orientation on surface characteristics of 5-axis milling", *Proceedings, 7th Annual Conference of Indonesian Aerospace Students in Europe and First Meeting of the Indonesian Marine Technology Students (IASE-7), Manchester, England, 12–14 July*, pp. E17–E28, 1995.
4. O. Kienzle, *Z. Ver, Dt. Ing.* 94, pp. 299–305, 1952.
5. A. J. P. Sabberwal, "Chip section and cutting force during the milling operation", *CIRP Annalen*, **10**, pp. 197–203, 1961.
6. W. A. Kline and R. E. DeVor, "The prediction of surface accuracy in end milling", *Journal of Engineering for Industry*, **104**, p. 272–278, *August* 1982.
7. A. E. Bayoumi, "An analytic mechanistic cutting force model for milling operations: a theory and methodology", *Journal of Engineering for Industry*, **116**, pp. 324–330, August 1994.
8. E. J. A. Armarego and N. P. Desphande, "Computerized end-milling force prediction with cutting models allowing for eccentricity and cutter deflections", *CIRP Annals*, **40** (1), pp. 25–29, 1991.
9. G. W. Vickers and K. W. Quan, "Ball-mills versus end-mills for curve surface machining", *Journal of Engineering for Industry*, **111**, pp. 22–26, February 1989.
10. J. P. Kruth and P. Klewais, "Optimization and dynamic adaptation of the cutter inclination during 5-axis milling of sculptured surface", *Annals of CIRP*, **43**(1), pp. 443–448, 1994.
11. H. Schulz and S. Hock, "High-speed milling of dies and moulds – cutting conditions and technology", *Annals of the CIRP*, **44** (1), pp. 35–38, 1995.
12. International Organization for Standardization, *ISO 3002: Basic Quantities in Cutting and Grinding*, 2nd edn, 1982.
13. J. Peters and P. Vanherck, "Machine tool stability test and the incremental stiffness", *Annals of the CIRP*, **17**, pp. 225–232, 1969.